https://doi.org/10.1093/brain/awae065 BRAIN 2024: 147; 2214–2229 | 2214

BRAIN
ORIGINAL ARTICLE

Macroscopic changes in aquaporin-4 underlie blast traumatic brain injury-related impairment in glymphatic function

Molly Braun,[1,2,3] Mathew Sevao,[1,2] Samantha A. Keil,[1,2] Elizabeth Gino,[1,2] Marie X. Wang,[1,2] Janet Lee,[4] Mariya A. Haveliwala,[1,2] Emily Klein,[1,2] Sanjana Agarwal,[1,2] Taylor Pedersen,[1,2] C. Harker Rhodes,[5,6,7] Deidre Jansson,[1,2] David Cook,[4,8] Elaine Peskind,[1,2] Daniel P. Perl,[6,7] Juan Piantino,[9] Abigail G. Schindler[1,2,4,8] and Jeffrey J. Iliff[1,2,10]

Mild traumatic brain injury (mTBI) has emerged as a potential risk factor for the development of neurodegenerative conditions such as Alzheimer's disease and chronic traumatic encephalopathy. Blast mTBI, caused by exposure to a pressure wave from an explosion, is predominantly experienced by military personnel and has increased in prevalence and severity in recent decades. Yet the underlying pathology of blast mTBI is largely unknown.

We examined the expression and localization of AQP4 in human post-mortem frontal cortex and observed distinct laminar differences in AQP4 expression following blast exposure. We also observed similar laminar changes in AQP4 expression and localization and delayed impairment of glymphatic function that emerged 28 days following blast injury in a mouse model of repetitive blast mTBI. In a cohort of veterans with blast mTBI, we observed that blast exposure was associated with an increased burden of frontal cortical MRI-visible perivascular spaces, a putative neuroimaging marker of glymphatic perivascular dysfunction.

These findings suggest that changes in AQP4 and delayed glymphatic impairment following blast injury may render the post-traumatic brain vulnerable to post-concussive symptoms and chronic neurodegeneration.

1 VISN 20 Northwest Mental Illness Research, Education and Clinical Center (MIRECC), VA Puget Sound Health Care System, Seattle, WA 98108, USA
2 Department of Psychiatry and Behavioral Sciences, University of Washington School of Medicine, Seattle, WA 98195, USA
3 Department of Neurosurgery, Medical College of Georgia, Augusta University, Augusta, GA 30912, USA
4 VISN 20 Geriatric Research, Education and Clinical Center (GRECC), VA Puget Sound Health Care System, Seattle, WA 98108, USA
5 Henry M. Jackson Foundation for the Advancement of Military Medicine Inc., Bethesda, MD 20817, USA
6 Department of Pathology, F Edward Hébert School of Medicine, Uniformed Services University of the Health Sciences, Bethesda, MD 20814, USA
7 DoD/USU Brain Tissue Repository, Uniformed Services University of the Health Sciences, Bethesda, MD 20814, USA
8 Department of Medicine, Division of Gerontology and Geriatric Medicine, University of Washington School of Medicine, Seattle, WA 98195, USA
9 Division of Child Neurology, Department of Pediatrics, Doernbecher Children's Hospital, Oregon Health & Science University, Portland, OR 97239, USA
10 Department of Neurology, University of Washington School of Medicine, Seattle, WA 98195, USA

Received September 22, 2023. Revised January 10, 2024. Accepted February 06, 2024. Advance access publication May 28, 2024
Published by Oxford University Press on behalf of the Guarantors of Brain 2024.

Correspondence to: Jeffrey J. Iliff
VISN 20 MIRECC, VA Puget Sound Healthcare System
1660 South Columbia Way, Seattle, WA 98108, USA
E-mail: jiliff@uw.edu

Keywords: traumatic brain injury; blast; glymphatic; aquaporin-4; perivascular space; sleep

Introduction

Traumatic brain injury (TBI) resulting from blast exposure, most often experienced by military personnel, has increased in incidence and severity in recent decades with the conflicts in Iraq and Afghanistan and the increasing use of improvised explosive devices (IEDs) in military conflicts. Strikingly, nearly half of all injured service members in the Iraq conflict experienced neurotrauma resulting from blast exposure.[1] In blast TBI, the energy from the explosion and resulting overpressure wave are transmitted through the brain, causing tissues of different densities such as grey and white matter to accelerate at different rates. This leads to the shearing and stretching of brain tissue, resulting in a diffuse pattern of tissue damage.[1,2]

Blast TBI shares strong clinical associations with post-traumatic stress disorder (PTSD), depression and persistent post-concussive neurobehavioural symptoms including sleep disruption and cognitive impairment.[3] Veterans with a history of TBI are more than twice as likely to die by suicide compared to veterans without a history of TBI.[4] Over the long term, blast TBI may increase the risk of neurodegenerative and dementing disorders such as Alzheimer's disease (AD) and chronic traumatic encephalopathy (CTE).[5] Despite these well-described associations, little is known about the mechanistic link between blast exposure and the development of these downstream neurological and psychiatric sequelae. One such mechanistic link may be impairment of the glymphatic system.

The glymphatic system is a brain-wide network of perivascular pathways along which CSF and interstitial fluid (ISF) exchange, supporting the clearance of interstitial solutes including amyloid-β,[6-8] tau[9,10] and α-synuclein.[11] Glymphatic exchange is anatomically organized, with CSF influx into the parenchyma driven by arterial pulsations along penetrating arteries[12,13] and directional flow through the brain parenchyma facilitated by the astroglial aquaporin-4 (AQP4) water channel localized to astrocytic endfeet lining perivascular spaces.[14] We previously reported in an experimental mouse model of impact TBI that glymphatic function is markedly and chronically impaired following TBI, and that this impairment is associated with the mislocalization of AQP4.[9,15] Several subsequent studies have reported impaired glymphatic function in rodent models of impact TBI.[16-20] Yet whether glymphatic function is impaired in the setting of blast TBI remains unknown.

A recent neuropathological report characterized a distinct pattern of astroglial scarring in the post-mortem human brain following blast exposure.[21] This characteristic 'interface astroglial scarring' was observed in brain tissue adjacent to CSF compartments including the cortical surface and ventricular wall, surrounding penetrating blood vessels and at the grey matter–white matter (GM-WM) interface. Based upon these changes, we hypothesized that AQP4 mislocalization may co-occur with this interface scarring, impairing glymphatic function. In this study, we assessed AQP4 expression and localization in post-mortem cortical tissue from a blast TBI human case series. We then evaluated whether similar changes in AQP4 expression and localization are observed in a mouse model of repetitive blast TBI and whether these changes are associated with impaired glymphatic function. We last evaluated whether blast TBI is associated with a higher burden of MRI-visible perivascular spaces (MV-PVSs), a putative marker of perivascular glymphatic impairment, in an observational cohort of veterans from the Iraq and Afghanistan conflicts.

Materials and methods

Human post-mortem histopathological study

Subjects

Brain specimens were acquired from the US Department of Defense Uniformed Services University (DoD/USU) Brain Tissue Repository at Uniformed Services University of the Health Sciences. For each case, written consent was obtained for donation of the brain for use in research. The brain tissue was collected, processed and stored and the associated clinical information obtained via procedures approved by the USU Institutional Review Board prior to the initiation of the study. All brains were extracted, handled and stored under the same conditions. Brains were taken at autopsy, placed into formalin and, after fixation, were sampled, embedded in paraffin and sectioned. The only variability was post-mortem interval (Supplementary Table 1), which was matched as much as possible across compared groups. All experiments followed federal, state, DoD and National Institutes of Health (NIH) guidelines and regulations for post-mortem analysis. Detailed subject information can be found in Supplementary Table 1.

Immunofluorescence for human post-mortem tissue

Paraffin-embedded tissue samples (5-μm thick formalin-fixed) from frontal cortex were examined from each case. Tissue was deparaffinized and treated with 10% formic acid, followed by antigen retrieval in acidic retrieval reagent (R&D Systems, Cat. No. #CTS014) in a steamer for 30 min. Sections were incubated in rabbit anti-AQP4 (1:500; Millipore Sigma; Cat. No. #AB3594) and mouse anti-GFAP (1:250; Millipore Sigma, Cat. No. #MAB360) diluted in 5% normal donkey serum in PBS with 0.3% Triton overnight at 4°C. Following overnight primary incubation, sections were incubated with secondary antibodies donkey anti-rabbit Alexa Fluor 488 (1:500; Invitrogen, Cat. No. #A21207) and donkey anti-mouse Alexa Fluor 594 (1:250; Invitrogen; Cat. No. #A21202) for 2 h at room temperature. Slices were mounted using ProLong™ Diamond Antifade Mountant with DAPI (Invitrogen, Cat. No. #P36971).

Quantification of AQP4 and GFAP in human tissue

Immunofluorescence (IF) imaging was performed on a Zeiss Aperio Scanscope FL fluorescent scanner with a 20×/0.75 Plan Apo objective. Micrographs were analysed using FIJI ImageJ software and the investigators were blinded to case status. Representative images in Fig. 1 were prepared using QuPath software.[22] For the laminar shell analysis, five concentric laminar regions of interest (ROIs)

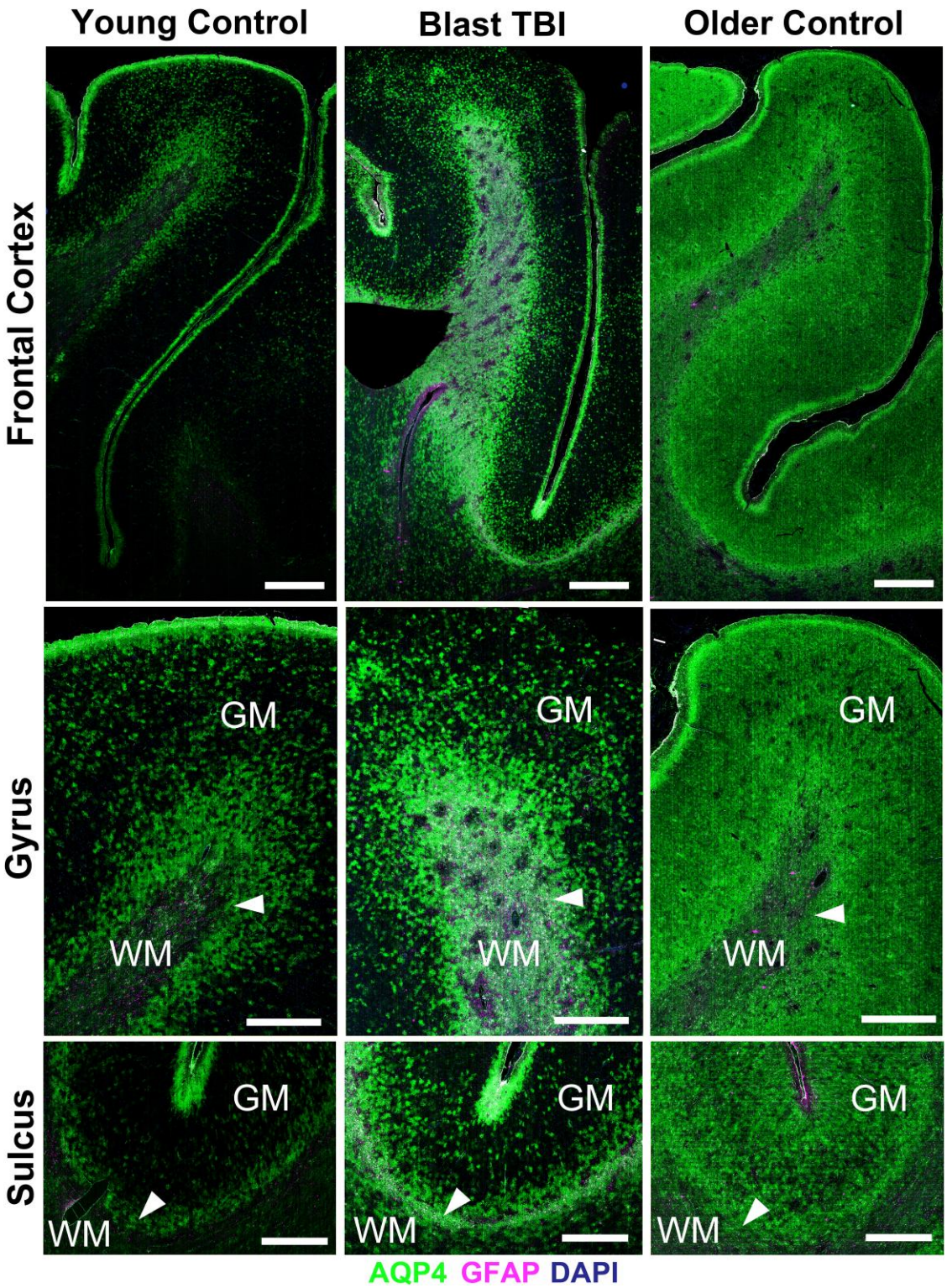

Figure 1 Altered AQP4 expression at the white matter–grey matter interface in human post-mortem blast tissue. Representative images of AQP4 and GFAP immunoreactivity in frontal cortex tissue from Young Control, Blast TBI and Older Control cases. Young Controls (19–37 years), Blast TBI (27–45 years), Older Controls (54–69 years), $n = 5$ per group. *Top*: Wide-field images extending from the crests of the gyri and depths of the sulci. High AQP4 and GFAP immunoreactivity at the white matter–grey matter interface and in the white matter of the Blast TBI case compared with Young or Older Controls, scale bar = 2 mm. *Middle*: Enlarged images of intensely immunoreactive astrocytes at the interface and white matter, scale bar = 1 mm. *Bottom*: Representative images at the depths of the sulci showing increased subpial and interface AQP4 labelling after blast injury, scale bar = 1 mm. Arrows indicate the junction between the white matter and grey matter. GM = grey matter; WM = white matter.

were drawn encompassing the superficial grey matter, middle grey matter, deep grey matter, superficial white matter and deep white matter. Mean intensity was measured for each shell ROI for both AQP4 and GFAP and normalized by dividing by the middle cortical shell value to account for autofluorescence in human post-mortem tissue. For area coverage, images were uniformly thresholded to derive the percentage of covered area for each ROI. For line analysis, linear ROIs were drawn across the tissue, from the pial surface, through the grey matter and into the white matter, to measure changes in AQP4 and GFAP immunofluorescence intensity. In each section, three linear ROIs were drawn each at the crest of the gyrus, midway down the gyrus and at the sulcal depth. The lines were realigned to the maximum intensity pixel of the first 4 pixels to start at the edge of the tissue. Replicate ROIs were averaged at each location for each case, and then averaged across groups. Given the variable distances across the grey and white matter between tissue samples, all lines were then scaled to a length of 1000 pixels and fit with a cubic spline function so that they were all the same length and were normalized by subtracting the average of pixels 200–400 (middle grey layer) of the line, serving as a baseline level of intensity. For analysis of AQP4 localization, linear radial ROIs were drawn outward from vessel walls through the surrounding vessel-associated astrocytes and surrounding neuropil. Pixel intensity projections were averaged within regions and within exposure groups to generate the average intensity projections. Vessels were considered to be capillaries if they were less than 10 μm in diameter, while those greater than 10 μm in diameter were considered 'large vessels'. Perivascular and non-perivascular segments of these linear ROIs were averaged and plotted. The first five pixels were averaged for the perivascular endfoot segment and the next 30 pixels were averaged for the non-perivascular segment. To define the 'polarization' of AQP4, we calculated the ratio of perivascular/non-perivascular AQP4 immunofluorescence by dividing the perivascular intensity by the non-perivascular intensities.

Rodent repetitive blast traumatic brain injury study

Rodent model of repetitive blast traumatic brain injury

Male C57Bl/6 mice were obtained from Jackson Laboratories and were 9 weeks of age at the time of arrival. Following 1 week of acclimation, mice were gently handled for at least 3 days prior to any experimental manipulations. Mice were allocated randomly by cage to different treatment groups. All animal experiments were conducted in accordance with the Association for Assessment and Accreditation of Laboratory Animal Care guidelines and approved by the VA Puget Sound Institutional Animal Care and Use Committees. Mice were anaesthetized with isofluorane (5% induction, 2%–3% maintenance), secured on a gurney and placed in a shock tube oriented perpendicular to the oncoming blast wave, so that their ventral body surface faced the oncoming shock wave. This shock tube (Baker Engineering and Risk Consultants) was designed to generate blast overpressure waves that mimic open-field high explosive detonations encountered by military service members in combat. Further details regarding the blast tube and shock wave generation have been described previously.[23,24] Mice underwent blast exposure once a day, every other day, for a total of three mild blast exposures over 5 days (~19 psi). Sham animals received the same amount of anaesthesia but were not exposed to a blast. After blast or sham exposure, mice were removed from the shock tube, anaesthesia was discontinued and mice were placed in a warm enclosure during recovery on a heated pad.

Intracisternal tracer infusion and imaging

Non-fixable infrared dye (LI-COR 800CW carboxylate, 100 nM; Fisher Scientific) and 0.5% fixable fluorescent Texas Red™ dextran (3 kD, TR-d3; Invitrogen) were combined in artificial CSF as the tracer. Ketamine/xylazine anaesthesia was used during the injection and imaging (intraperitoneal; 130 mg/kg ketamine, 8.8 mg/kg xylazine, 0.02 ml/g body weight). Thirty minutes after the initial dose, a one-third dose of ketamine/xylazine by weight was administered to maintain the plane of anaesthesia. The order of tracer infusion was randomized by cage and the surgeon was blinded to treatment status. Mice were fixed in a stereotaxic frame, the dura mater was exposed via dissection of the neck muscles below the occipital crest and a 30G steel needle was inserted 1–2 mm into the cisterna magna through the atlanto-occipital membrane. The cannula was secured to the dural membrane with cyanoacrylate glue and 10 μl of dual CSF tracer was injected over 10 min with a syringe pump (Harvard Apparatus). Mice were placed on a heated LI-COR Pearl imager platform to image transcranial movement of the infrared dye every 2 min from 20 min to 42 min post tracer injection.[25] Mice were imaged starting at 20 min post injection due to constraints from the imaging platform being enclosed. At 45 min, the mice were transcardially perfused with chilled PBS and 4% paraformaldehyde (PFA). Brains were extracted and LI-COR images were taken of the dorsal brain surface.

LI-COR dynamic and surface analysis

Circular ROIs were drawn over each cortical hemisphere of the 12 transcranial LI-COR images and intensity was measured. Both sides were then averaged and plotted over time. For dorsal surface images, ROIs were drawn for each dorsal cortex hemisphere, intensity was measured and both sides were averaged.

Tracer slice imaging and analysis

Brains were post-fixed in 4% PFA overnight at 4°C, rinsed in PBS, cryoprotected in 30% sucrose and embedded in optimal cutting temperature compound (O.C.T.). Brains were sectioned coronally on a cryostat at a thickness of 20 μm. Three sections located at +0.25, −1.25 and −2.75 from bregma were mounted with ProLong™ Diamond Antifade Mountant with DAPI (Invitrogen, Cat. No. #P36971) and imaged on a Keyence BZ-X800 fluorescence scope. Researchers performing imaging were blinded to treatment status. Tile scans were taken at 10× magnification and images were stitched and saved as TIFF files for analysis. Regional ROIs were drawn for the dorsal cortex, ventral cortex, corpus callosum, hippocampus and subcortical region, and mean intensity was measured to quantify influx of TR-d3. Tissue was excluded if it was cut at an angle where it could not be matched anatomically or too torn or damaged for accurate analysis.

Immunofluorescence for rodent tissue

Frozen sections from the tracer experiments were also used for immunofluorescence. Sections were incubated in rabbit anti-AQP4 (1:500; Millipore Sigma, Cat. No. #AB3594) or anti-GFAP (1:250; Millipore Sigma, Cat. No. #MAB360) diluted in 5% normal donkey serum in PBS with 0.3% Triton overnight at 4°C. Following overnight primary incubation, sections were incubated with secondary antibodies donkey anti-rabbit Alexa Fluor 647 (1:500; Invitrogen, Cat. No. #A21207) and DyLight 488-labelled *Lycopersicon esculentum* (Tomato) lectin (Vector Labs, Cat. No. #DL-1177) or donkey anti-mouse Alexa Fluor 488 (1:250; Invitrogen, Cat. No. #A21202) for 2 h

at room temperature. Slices were mounted using ProLong™ Diamond Antifade Mountant with DAPI (Invitrogen, Cat. No. #P36971).

Quantification of AQP4 and GFAP in rodent tissue

Researchers performing image analysis were blinded to treatment status. For the shell analysis, three concentric laminar ROIs were drawn encompassing the superficial grey matter, deep grey matter and white matter for each hemisphere. Mean AQP4 intensity was measured for each shell ROI and matching hemisphere ROIs were averaged. For the line analysis, a linear ROI was drawn across the dorsal cortex, from the pial surface, through the grey matter and into the white matter of each hemisphere, and then averaged. A linear ROI was also drawn on the ventral surface of each hemisphere from the brain surface through the grey matter. These linear ROIs were then averaged for both sides. For AQP4 localization analysis, a vessel mask was generated in Fiji (ImageJ) using lectin vessel staining. The AQP4 image was subtracted from the lectin mask image to measure the AQP4 associated with the vasculature or perivascular AQP4 intensity. The same process was performed using the inverted mask to measure non-perivascular AQP4 intensity. The image was thresholded to remove pixels below zero and the mean intensity was measured within square ROIs placed in areas of interest. A 'polarization' ratio was calculated by dividing perivascular intensity by non-perivascular intensity. For GFAP analysis, regional ROIs were drawn and mean intensity, uniform thresholded intensity and percentage of covered area were measured. Tissue was excluded if it was cut at an angle where it could not be matched anatomically or if tissue was too torn or damaged for accurate analysis.

Activity and sleep measures using the Comprehensive Lab Animal Monitoring System

Activity patterns were assessed using the Columbus Instruments Comprehensive Lab Animal Monitoring System (CLAMS). Mice were individually housed in the CLAMS for five consecutive days, 4 weeks following the final blast with *ad libitum* food and water, and cages were placed so that the location of treatment groups was alternated. Activity was measured in the CLAMS using infrared beam break, and 'sleep' was classified as any epoch with no movement (each epoch was 60 s) as previously described[26] and validated with simultaneous recordings of EEG. Data from the first 24 h in the CLAMS were excluded to remove the potential confounding initial stress of single housing in the CLAMS unit. Activity was assessed following mild repetitive blast (or sham) exposure once a day for 3 days, for a total of three mild blast exposures (~19 psi). Data processing and visualization was conducted in Python using standard scientific computing libraries (Pandas, Seaborn). Additional circadian rhythm analysis was conducted using Python implementations (RhythmCount[27] and CosinorPy[28]) of cosinor-based methods for rhythmicity detection and analysis. No animals were excluded.

Human MRI study

Study participants

We performed an analysis of MRI in Operation Enduring Freedom/Operation Iraqi Freedom/Operation New Dawn (OEF/OIF/OND) veterans. The study was approved by the VA Puget Sound and Oregon Health and Science University Institutional Review Boards. All subjects provided informed consent before study enrolment. The details of the study enrolment and follow-up are detailed elsewhere.[29,30] Subjects were enrolled between March 2011 and September 2019. Subjects were included in this analysis if they reported a history of mild TBI (due to blast or any other cause) and had MRI data available for MRI-visible perivascular space (MV-PVS) segmentation, resulting in 56 veterans with a history of blast-related mild TBI (mTBI) used in this study. Mild TBI was defined as per the American Congress of Rehabilitation Medicine diagnostic criteria, i.e. one or more of the following was present: (i) loss of consciousness up to 30min; (ii) loss of memory for events surrounding the event for up to 24 h; or (iii) any alteration in mental state. Exclusion criteria included: a neurological disorder (including moderate or severe traumatic brain injury), lifetime diagnoses of schizophrenia, other psychotic disorder or bipolar disorder, or a diagnosis of substance abuse or dependence within the past 3 months. MRI subjects were a separate cohort of veterans from the brain specimens used for the histological evaluation.

Assessment of mild traumatic brain injury and sleep

Lifetime history of both blast and impact mTBI was obtained as previously described.[30-32] Briefly, two trained study members performed a semi-structured interview of each study subject and obtained detailed information regarding each lifetime event that met mTBI criteria, including characteristics (blast versus impact), duration of loss of consciousness and sequela. The total number of mTBIs sustained in the military was used for analysis. Sleep was assessed with the Pittsburgh Sleep Quality Inventory (PSQI). The PSQI measures sleep symptoms over the previous month and provides an overall sleep quality score ranging from 0 to 21. A global score of ≥5 is commonly used to qualify poor sleep.[33]

MRI acquisition, imaging processing and perivascular space segmentation

The methods for MRI acquisition, processing and MV-PVS segmentation in this cohort are described elsewhere.[32,34,35] Briefly, sagittal 3D T1-weighted images [repetition time (TR)/echo time (TE)/inversion time (TI) = 7.6/3.5/909 ms, imaging matrix = 256 × 256 × 176, resolution =1 × 1 × 1 mm] and fluid-attenuated inversion recovery (FLAIR; TR/TE/TI = 4800/245/1650 ms, imaging matrix = 168 × 168 × 120, resolution 1 × 1 × 1.5 mm) MRI were collected on a 3.0 T Philips Achieva whole-body scanner (Philips Medical Systems). White matter masks were obtained via FreeSurfer (version 5.1) and eroded by a single voxel to avoid potential partial volume effects. MV-PVS segmentation was obtained using a previously described method[34,35] that identifies white matter T1 hypointense PVSs based on prespecified morphological criteria. The algorithm output is then assessed by a blinded researcher and false calls are removed from the mask. Based on previous studies, the PVS detection algorithm has a false positive detection rate of 19.4% (i.e. 19.4% of the clusters detected are not PVSs).[36] Those are removed by manual inspection, so the final data contain only true positive PVSs.

Statistical analysis

Human post-mortem tissue and rodent studies

All data were analysed using GraphPad Prism 9 software. Two group comparisons were analysed by two-sided *t*-test. Multi-group comparisons were made using a one-way, two-way or two-way repeated measures ANOVA where appropriate. Mixed effects analyses were used when values were missing or to control for correlation within subjects. A *P*-value of <0.05 was considered to

be significant. Sample sizes were determined by previous experience.

Human MRI

Statistical analysis was performed using Stata/MP software (version 15; Stata Corp LP, College Station, TX). Descriptive statistics were used to summarize the cohort's characteristics. The primary outcome was MV-PVS burden, defined as two separate outcome variables: MV-PVS number (the number of PVSs per cm^3 of white matter) and volume [the total volume of PVS (mm^3) per cm^3 of white matter]. The primary exposure was the number of mTBIs sustained in the military. Potential predictors and confounders were: age, systolic blood pressure and self-reported sleep (dichotomous, based on PSQI parameters).[33] The association between MV-PVS burden and number of mTBIs after adjusting for the above-mentioned covariates was analysed with multivariate regression. We also examined poor sleep as a potential effect modifier (interaction) of the association between MV-PVS burden and the number of mTBIs. Assumptions of normality, linearity and homoscedasticity were tested with residual versus fitted plots and quantile-quantile plots. Multi-collinearity was tested by calculating correlation coefficients and variance inflation factors. Normality was assessed with the Shapiro–Wilk test. MV-PVS number and volume are not normally distributed, and therefore they were log-transformed. We report *P*-values as well as 95% confidence intervals. All reported *P*-values are two-sided and the threshold for statistical significance was set to an alpha of 0.05.

Results

Laminar changes in AQP4 expression in the human post-mortem blast-injured brain

We first sought to define whether the interface glial scarring described in the human post-mortem brain following blast TBI exposure was associated with alterations in AQP4 expression and localization. AQP4 expression and localization were evaluated in post-mortem frontal cortical specimens from a case series including five 'Young Control' cases (19–37 years of age) with no history of TBI, five 'Blast TBI' cases (27–45 years of age) and five 'Older Control' cases (54–69 years of age) with no history of TBI from the Neuropathology Core at Uniformed Services University of the Health Sciences. All cases, including controls, were former military service members. Demographic and clinical characteristics of the cases are detailed in Supplementary Table 1. Of note, many of these cases had psychiatric disorders and/or died by suicide, which may have influenced our neuropathological findings. Wide-field images in Fig. 1 depict macroscopic laminar differences in immunofluorescence of the astroglial marker GFAP and AQP4 between Young Control, Blast TBI and Older Control cases. As previously reported,[21] compared with Young Control cases, the Blast TBI cases exhibited prominent astroglial scarring, as evidenced by increased GFAP immunofluorescence at the pial surface, at the GM-WM interface and within the subcortical white matter (Fig. 1). In parallel, we also evaluated frontal cortical AQP4 expression and observed a similar pattern of increased AQP4 immunofluorescence, particularly at the GM-WM interface and in the subcortical white matter (Fig. 1), compared with that observed in Young Controls. Older Controls varied in their AQP4 immunofluorescence but tended to have a more uniform AQP4 expression throughout the grey matter. Note that the representative Blast TBI images in Fig. 1 lack the intense subpial AQP4 immunofluorescence due to the tissue cutting process; however, intense subpial AQP4 immunofluorescence was seen on adjacent gyri and at the depth of the sulcus shown.

To quantify these macroscopic laminar patterns of AQP4 and GFAP expression, AQP4 and GFAP immunofluorescence were evaluated across five concentric laminar ROIs, including superficial grey matter, middle grey matter, deep grey matter, superficial white matter and deep white matter (Fig. 2A). Linear regression analyses showed that increasing AQP4 immunofluorescence was significantly associated with increasing GFAP immunofluorescence across all layers ($P < 0.0002$, $R^2 = 0.22$; Supplementary Fig. 1), suggesting a relationship between the previously described[21] interface astroglial scarring and these laminar changes in AQP4 expression. We observed significant laminar differences in AQP4 immunofluorescence across groups (main effects of Layer, $P < 0.0001$; Group, $P < 0.01$; and Layer × Group interaction, $P < 0.0001$). Specifically, within the superficial and middle grey matter, AQP4 immunofluorescence was similar across all three groups. However, AQP4 immunofluorescence was higher in Blast TBI cases at the GM-WM boundary and within the superficial ($P < 0.01$) and deep white matter ($P < 0.05$; Fig. 2B). A similar pattern was observed for normalized GFAP expression through the depth of the tissue (main effects of Layer, $P < 0.0001$; Layer × Group interaction, $P < 0.05$; Fig. 2C). To capture the laminar profiles of AQP4 and GFAP expression more granularly and to compare differences along the length of the gyri, linear ROIs were drawn across the tissue, from the pial surface, through the grey matter and into the white matter. In each section, three linear ROIs were drawn each at the crest of the gyrus, midway down the gyrus and at the sulcal depth. The immunofluorescence intensity was averaged across replicate ROIs at each location for each subject, then averaged across groups (Supplementary Fig. 2A). While more subtle differences in AQP4 and GFAP profiles were seen across the tissue at the crests of the gyri (Supplementary Fig. 2B) and midway between the crests of the gyri and depths of the sulci (Supplementary Fig. 2C), the most pronounced differences in profiles were observed at the sulcal depths, where intense AQP4 and GFAP immunofluorescence was observed in subpial layers and both at the GM-WM boundary and within the deeper white matter (Fig. 2E and Supplementary Fig. 2D). We detected main effects of Depth ($P < 0.0001$) and Depth × Group interactions ($P < 0.0001$) in the superficial grey matter, deep grey matter and superficial white matter for AQP4 immunofluorescence. Main effects of Depth ($P < 0.0001$) in the middle grey matter and Group in the deep white matter ($P < 0.05$) were also observed. For GFAP immunofluorescence, interaction effects of Depth × Group ($P < 0.05$) were observed in the middle grey matter and deep grey matter; a main effect of Group ($P < 0.05$) was observed in the superficial white matter. Overall, macroscopic laminar changes in AQP4 and GFAP were observed in the Blast TBI cases, with the greatest changes found in subpial regions, at the sulcal depth, at the GM-WM boundary and in the deeper white matter.

Changes in perivascular AQP4 localization in the human blast-injured brain

Next, we evaluated AQP4 intensity and localization at the level of perivascular astroglial endfeet surrounding capillaries and larger intraparenchymal blood vessels in the superficial grey matter, middle grey matter, GM-WM boundary and deep white matter (Supplementary Figs 3–5). To quantify perivascular AQP4 expression and localization, linear radial ROIs were drawn outward from vessel walls, through the surrounding vessel-associated astrocytes

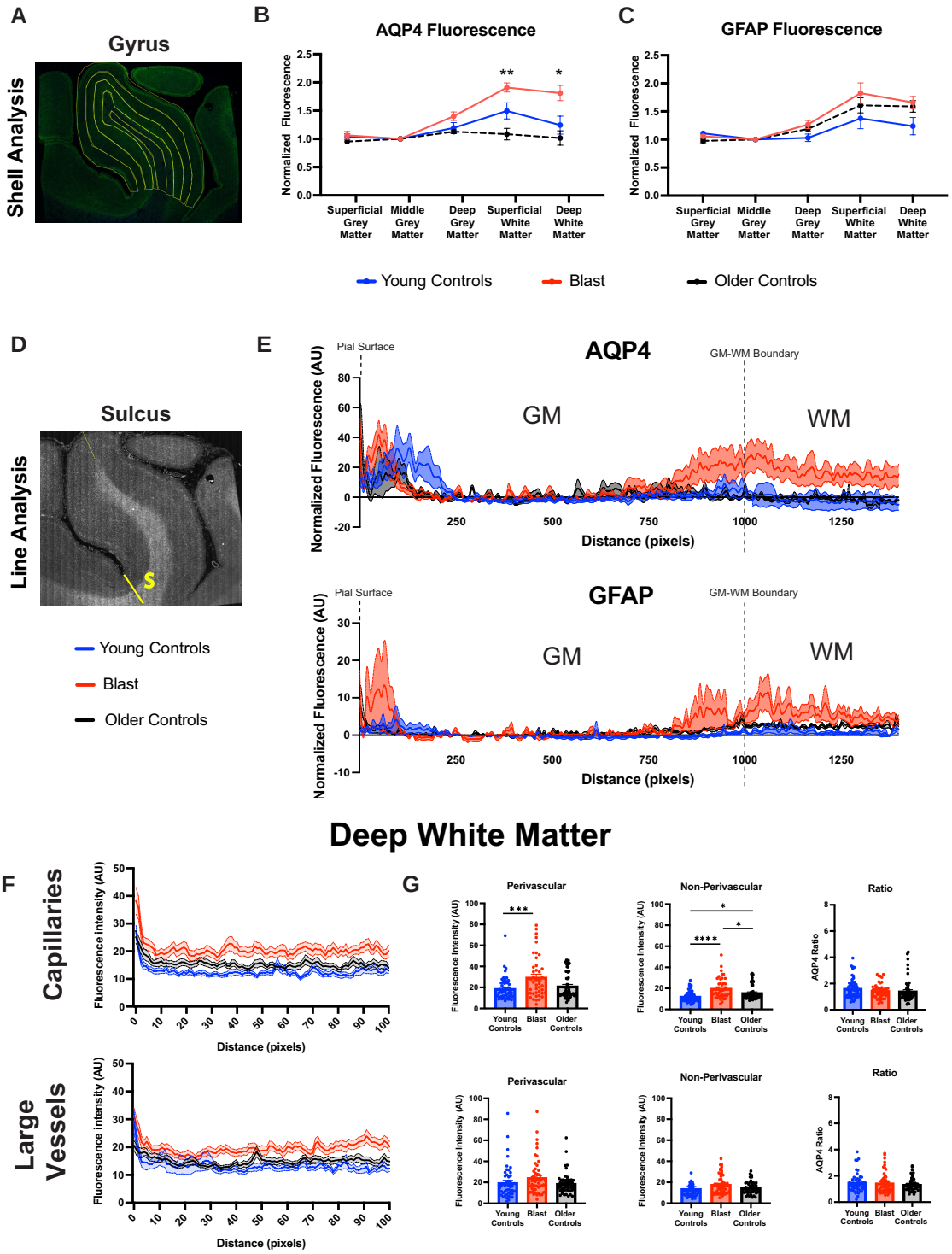

Figure 2 Laminar differences in GFAP and AQP4 immunoreactivity in human blast TBI. (**A**) Representative image of the five laminar regions of interest (ROIs) analysed, with the outermost ROI being the superficial grey matter, followed by the middle grey matter, deep grey matter, superficial white matter and the innermost ROI, the deep white matter. (**B**) Quantification of AQP4 and (**C**) GFAP across grey and white matter layers expressed as normalized mean fluorescence intensity. Data are mean ± SEM from $n = 5$ per group and were analysed with two-way repeated measure ANOVA followed by Sidak's *post hoc* test ($^{*}P < 0.05$, $^{**}P < 0.01$ for Blast versus Older Controls). (**D**) Representative image of drawn line ROI extending from the cortical surface into the subcortical white matter to generate intensity projection plots of GFAP and AQP4 across the tissue at the sulcus (S). (**E**) Averaged intensity plots of normalized fluorescence intensity of AQP4 and GFAP at the sulcal depth are shown for $n = 5$ cases per group. Increased GFAP and AQP4 was observed at the white matter–grey matter interface and throughout the white matter in blast-injured post-mortem human brain tissue. (**F** and **G**) Averaged fluorescence intensity plots of AQP4 immunostaining surrounding capillaries and large vessels. Vessel diameter was measured and lines were drawn through the perivascular endfoot, continuing through the surrounding astrocytes and parenchyma. Both intensity projection plots were averaged for a single intensity plot per vessel and then averaged across groups. (**F**) Quantification of binned AQP4 intensity plot segments surrounding capillaries and large vessels at the junction of the white matter and grey matter. For graphing of perivascular and non-perivascular segments, the first five pixels were averaged for the perivascular endfoot segment and the next 30 pixels were averaged for the non-perivascular segment. Data are mean ± SEM from an average of 7–10 vessels per vessel type, per region, per case. Data were analysed with mixed effect analysis followed by Sidak's *post hoc* test to control for within case correlation ($^{*}P < 0.05$, $^{**}P < 0.01$, $^{***}P < 0.001$,$^{****}P < 0.0001$). GM = grey matter; WM = white matter.

and surrounding neuropil (Supplementary Figs 4A and 5A). Pixel intensity projections were averaged within regions and within exposure groups to generate the average intensity projections shown in Fig. 2F and Supplementary Fig. 4B–E. Vessels were considered to be capillaries if they were less than 10 µm in diameter between vessel walls, while those greater than 10 µm in diameter were considered 'large vessels'. In the superficial grey matter, there was an overall main effect of Group for AQP4 intensity for capillaries ($P < 0.05$) and Distance × Group interaction for large vessels ($P < 0.0001$). In the middle grey matter and deep grey matter/superficial white matter, there was no significant main effect of Group for either vessel type, but there was a Distance × Group interaction for both capillaries ($P < 0.0001$, middle grey matter; $P < 0.0001$, deep grey matter/superficial white matter) and large vessels ($P < 0.0001$, middle grey matter; $P < 0.05$, deep grey matter/superficial white matter). In the deep white matter, there was a main effect of Group for AQP4 intensity for both capillaries and large vessels ($P < 0.0001$). These data demonstrate that the profiles of AQP4 immunofluorescence surrounding cerebral blood vessels may have been substantially altered by blast TBI exposure.

To compare different astroglial domains across groups, perivascular and non-perivascular segments of these linear ROIs were averaged and plotted. To define the relative perivascular 'polarization' of AQP4, we calculated the ratio of perivascular/non-perivascular AQP4 immunofluorescence. The complete characterization of AQP4 immunofluorescence and AQP4 polarization for capillaries and large vessels in the superficial grey matter, middle grey matter, GM-WM boundary and deep white matter are provided in Supplementary Fig. 5A–E. The most consistent and pronounced differences were observed in association with the capillaries in the middle grey matter and GM-WM boundary regions, which we further divided into deep grey matter/superficial white matter (Supplementary Fig. 5C and D) and deep white matter (Fig. 2G and Supplementary Fig. 5E). Generally, both capillary-associated perivascular and non-perivascular AQP4 immunofluorescence were increased in Blast TBI cases compared to Young Control or Older Control cases. Because AQP4 immunofluorescence was increased in both perivascular and non-perivascular segments of Blast TBI cases, the derived AQP4 polarization measure did not differ by group. In total, these data from a post-mortem case series suggest that blast TBI in humans is associated with pronounced laminar increases in AQP4 expression but with more subtle changes in perivascular AQP4 localization.

AQP4 changes in a murine model of mild repetitive blast traumatic brain injury

We next sought to evaluate whether changes in AQP4 expression and localization observed after blast TBI resulted in functional impairment of perivascular glymphatic function. To do this, we examined AQP4 expression and glymphatic function in a mouse model of repetitive blast mTBI. Evaluating AQP4 immunofluorescence at 7 and 28 days post-blast mTBI, we observed delayed macroscopic changes in AQP4 expression at 28 days post-blast (Fig. 3A), with prominent enhancement of AQP4 immunofluorescence at the cortical brain surface (Fig. 3B). Mean AQP4 immunofluorescence intensity was quantified in superficial grey matter, deep grey matter and subcortical white matter 'shell' ROIs. Mean AQP4 immunofluorescence was also measured along linear ROIs spanning the pial surface through the subcortical white matter (Fig. 3C). Laminar shell-based analysis demonstrated that AQP4 immunofluorescence was significantly increased in the superficial grey matter of the cortex at 28 days compared with 7 days post-blast ($P < 0.05$) and sham ($P < 0.05$) (Fig. 3D). There was also a trend in increased AQP4 intensity in the white matter, however this change was not significant. Linear ROI analysis from the dorsal cortical surface, through the grey matter and into the subcortical white matter showed increased AQP4 immunofluorescence intensity at the cortical surface at 28 days compared with 7 days post-blast mTBI and sham brains (Fig. 3E). AQP4 expression was also elevated at 28 days post-blast mTBI at the GM-WM boundary and in the subcortical white matter. Similar results were observed in ventral cortical linear ROIs at 28 days compared with 7 days post-blast mTBI (Fig. 3F). To assess perivascular AQP4 localization, we conducted co-staining with lectin to label blood vessels. Vessel masks were generated from the lectin images in rectangular ROIs and AQP4 fluorescence intensity was quantified within perivascular and non-perivascular pixels (Supplementary Fig. 6A). From these measures we also computed a perivascular/non-perivascular AQP4 'polarization' ratio. In general, we observed that at 28 days post-blast mTBI, non-perivascular AQP4 immunofluorescence tended to increase (Fig. 3G and H and Supplementary Fig. 6B–E), while the AQP4 polarization tended to decline. However, these effects only reached significance for increasing non-perivascular AQP4 immunofluorescence in the ventral cortex, striatum and hypothalamus ($P < 0.05$). Subcortical white matter ($P < 0.05$, 28 days versus 7 days post-blast) and grey matter ($P < 0.01$, 28 days versus 7 days post-blast, 28 days post-blast versus sham) GFAP immunofluorescence increased at 28 days post-blast mTBI, although this reactive astrogliosis was relatively subtle (Supplementary Fig. 7). These findings demonstrate similar alterations in AQP4 expression and localization occur in a murine model of repetitive blast mTBI to those observed in post-mortem cases from veterans with a history of blast TBI, as evidenced by the macroscopic and microscopic (perivascular/non-perivascular) increases in AQP4 that were observed.

Delayed impairment in glymphatic function and sleep-wake disruption following murine blast mTBI

We next examined whether changes in AQP4 localization associated with blast TBI resulted in impairment of glymphatic function. To do this, we conducted paired dynamic infrared and fixed-slice fluorescence CSF tracer studies in mice exposed to repetitive blast mTBI. Two tracers (IRDye and TRd3) were injected into the cisterna magna at either 7 or 28 days following the third and final blast injury or sham procedure. Infrared tracer movement was imaged transcranially, every 2 min on a LI-COR Pearl Trilogy small animal imaging system, between 20 and 42-min post-injection and then the animals were perfusion-fixed and infrared imaging was performed on the fixed, extracted brains. Dynamic transcranial imaging showed slower CSF tracer accumulation for both 7 and 28 days post-blast mTBI compared with sham (Fig. 4A; main effects of Time, $P < 0.0001$; Time × Treatment interaction, $P < 0.001$). Mean infrared fluorescence intensity was significantly decreased at the dorsal surface at 28 days post-blast mTBI compared with sham ($P < 0.05$; Fig. 4B and C). Brains were then sectioned coronally and three brain slices, as shown in relation to bregma (Fig. 4D), were further analysed to assess fixable fluorescent CSF tracer influx into the dorsal cortex, ventral cortex, corpus callosum, hippocampus and subcortical ROIs (Fig. 4E and F). CSF tracer influx was significantly reduced in the dorsal cortex at 28 days compared with 7 days post-blast mTBI ($P < 0.01$; Fig. 4G) and sham ($P < 0.01$) and in the ventral cortex at 28 days compared with 7 days post-blast mTBI ($P < 0.05$) and sham ($P < 0.01$)

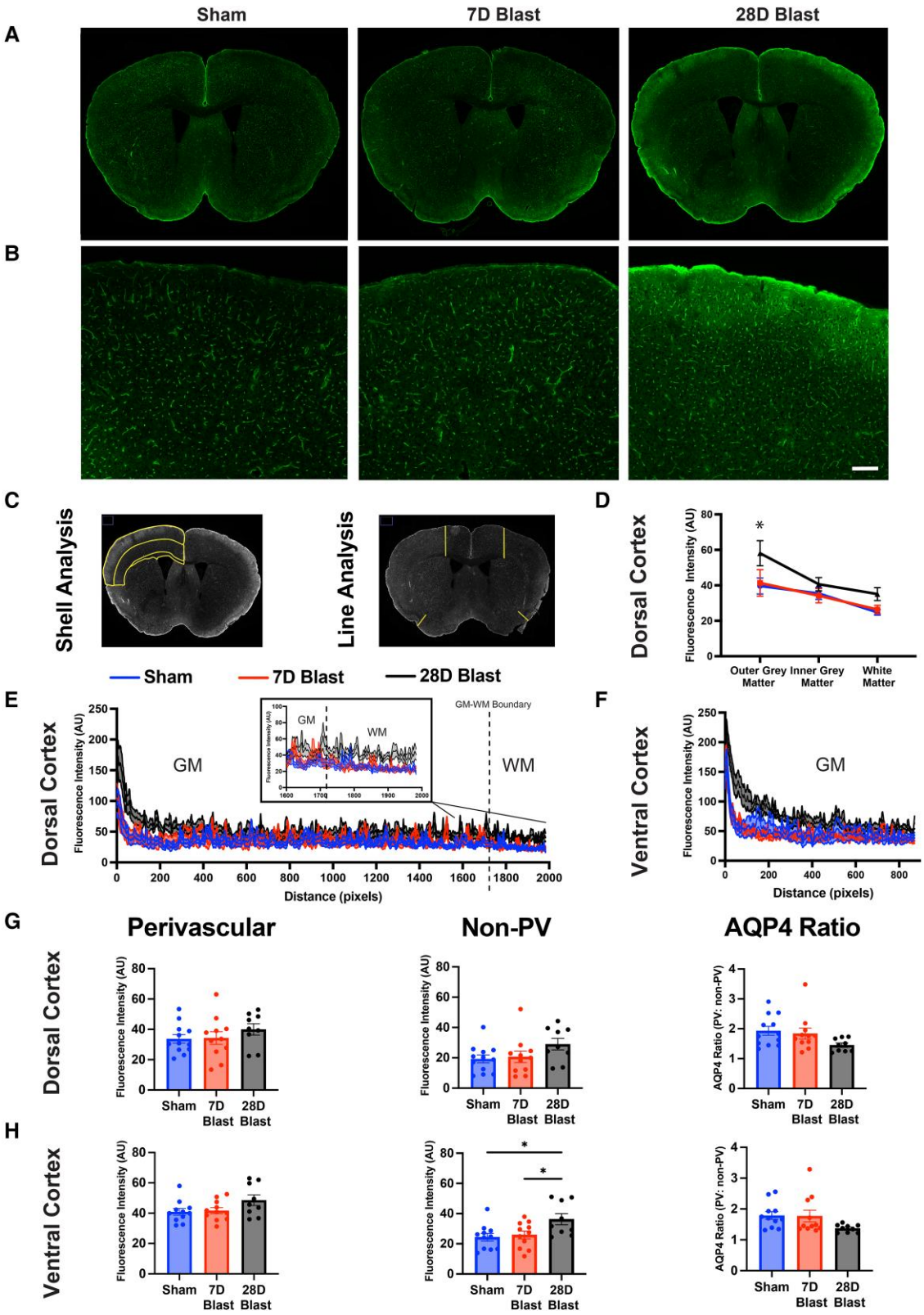

Figure 3 Increased AQP4 in the murine brain following mild repetitive blast traumatic brain injury. (**A**) Representative whole brain slice images of AQP4 immunostaining in mouse brains of Sham group and 7 (7D Blast) and 28 days (28D Blast) post mild repetitive blast traumatic brain injury (mTBI). (**B**) Representative dorsal cortex images of AQP4 immunostaining in Sham, 7D Blast and 28D Blast mouse brains. Scale bar = 200 μm. Increased AQP4, particularly at the cortical surface, was observed at 28 days post mTBI. (**C**) Representative images of the regions of interest drawn for regional shell analysis of AQP4 in outer grey, inner grey and white matter and representative dorsal and ventral lines drawn for AQP4 line analysis generate intensity plots of AQP4 across the tissue. (**D**) AQP4 fluorescence intensity from regional shell analysis showing AQP4 immunoreactivity was

(Continued)

(Supplementary Fig. 8). No significant differences were observed in tracer influx in the corpus callosum, hippocampus and subcortical ROIs (Supplementary Fig. 8).

Given that glymphatic function is more active during sleep[8] and is regulated by the circadian cycle,[37] we next examined circadian activity patterns in sham and blast mTBI mice by cosinor-based rhythm assessment (RhythmCount) using raw activity count data measured over 72 h in the CLAM system, 4 weeks after the final blast (Fig. 4H). These rhythm shifts indicate dark period (typical period of wake for rodents) sleepiness and light period (typical period of sleep for rodents) insomnia following repetitive blast. A heat map of activity across time shows differences in hourly activity levels between blast mTBI and sham mice (Fig. 4I). An additional cosinor-based rhythm assessment was performed using CosinorPy, showing a subtle decrease in amplitude (Fig. 4J) and a shift in acrophase (the peak of the rhythm cycle) following blast mTBI (Fig. 4K). Total dark period sleep and percentage sleep per hour were significantly increased following blast ($P < 0.05$), with 10.6% and 10.8% increases, respectively, while sleep bout counts per hour remained unchanged (Fig. 4L). In total, these findings demonstrated that experimental murine blast mTBI results in chronically impaired glymphatic function as well as in the emergence of sleep-wake disruption similar to those observed clinically in veterans following blast TBI.

Effect of blast traumatic brain injury on lobar subcortical MRI-visible perivascular spaces

We last evaluated whether blast mTBI is associated with evidence of glymphatic impairment in living veterans with a history of experiencing these events. MV-PVSs within the subcortical white matter have emerged as putative markers of perivascular dysfunction in human populations.[32,38] We conducted MV-PVS segmentation on MRI data from 56 OEF/OIF/OND veterans with a self-reported history of blast mTBI (Supplementary Table 2).[34] Sleep quality was also assessed with the PSQI, which measures symptoms of sleep disturbances over 1 month and results in a global score ranging from 0–21. Participants with a global PSQI score ≥5 are considered to be poor sleepers.[33] The number of MV-PVSs was positively associated with the number of mTBIs experienced in both the frontal ($P < 0.05$) and parieto-occipital lobes ($P < 0.05$) (Fig. 5A and B and Table 1). The volume of MV-PVSs was also positively associated with the number of mTBIs in the frontal lobe ($P < 0.05$) (Table 1). We detected an interaction effect between the number of mTBIs, sleep quality and MV-PVS number and volume in the frontal lobe ($P < 0.05$), suggesting that sleep quality modulates the relationship between the number of mTBIs and MV-PVS number and volume. In subjects who reported poor sleep, the increase in PVS volume observed with each subsequent mTBI was higher than in those who reported good sleep (Table 1). These data showed, in a clinical population of veterans, that blast mTBI is associated with a putative marker of perivascular glymphatic dysfunction, MV-PVS burden and that this relationship is intensified among those reporting poor sleep.

Discussion

This study is the first to characterize AQP4 expression and localization and glymphatic function following blast mTBI across both an experimental rodent model of blast mTBI as well as in the setting of human clinical blast mTBI. We observed widespread macroscopic changes in AQP4 expression in blast-exposed human postmortem tissue that was mirrored in a mouse model of repetitive blast injury. These changes in AQP4 localization were associated with delayed glymphatic impairment within our experimental rodent model, while in living military veterans with a history of blast mTBI, MV-PVSs (putative markers of glymphatic function) were associated with blast mTBI and poor sleep.

Studies in rodent models demonstrate that glymphatic exchange contributes to the clearance of amyloid-β and tau, while its experimental impairment is sufficient to promote the development of amyloid-β and tau pathology.[6,8,9,39-41] Thus, impairment of glymphatic function may represent a key mechanistic link underpinning the clinical relationship between TBI and the neuropathology underlying AD and CTE. However, the linkage between blast TBI and these features has proven complex, as evidenced by previous literature on the topic. In prior studies, two human postmortem blast cases from the wider case series lacked tau pathology, with few blast TBI cases showing evidence of scant tau pathology and even fewer with neurofibrillary tangles and tau immunoreactivity consistent with CTE.[21,42] This is consistent with another human case series that found no evidence of tau pathology among cases with blast TBI.[43] Another small case series and a case study, however, did report CTE-like tau pathology following blast TBI.[44,45] A caveat to these studies is that some of the cases had a history of participation in contact sports, which could underlie the observed tau pathology. A wider case series also lacked amyloid plaque pathology,[21] although a honeycomb pattern of amyloid precursor protein immunoreactivity throughout the subcortical white matter, consistent with diffuse axonal injury, has been reported following blast TBI exposure.[43] These findings suggest that tau and amyloid-β pathology may not be consistent neuropathological hallmarks of blast TBI. An important limitation to these studies and our understanding of the relationship between blast TBI, AD and CTE, however, is the relatively brief interval (years, rather than decades) between blast events and death in many of these cases. The amyloid-β and tau pathology associated with both AD and CTE are believed to arise over the course of many years or even decades. However, with the recency of the conflicts in Iraq and Afghanistan, most neuropathological cases with blast TBI have tended to be fairly young, with a relatively short interval between the blast TBI and death. Based on these factors, it is difficult to ascertain whether AD- and CTE-related amyloid-β and tau pathology are simply not clinically associated with blast

Figure 3 Continued
significantly increased in the outer grey matter at 28 days post mTBI. Data are mean ± SEM from $n = 8$–10 per group and were analysed with two-way repeated measure ANOVA followed by Sidak's *post hoc* test (*$P < 0.05$, 28 days versus 7 days post mTBI; *$P < 0.05$, 28 days post mTBI versus Sham). (**E**) Averaged fluorescence intensity plots from the dorsal surface through the grey matter (as shown in **D**) and into the subcortical white matter. Data are mean ± SEM from $n = 9$–10 mice/group. (**F**) Averaged fluorescence intensity plots extending from the ventral surface through the grey matter (as shown in **D**) for $n = 9$ per group. (**G**) Quantification of AQP4 expression and localization in the dorsal cortex. AQP4 was co-stained with lectin to label blood vessels, a vessel mask was generated and AQP4 fluorescence intensity was measured inside or outside the vessel mask to quantify perivascular (PV) and non-PV AQP4, respectively. AQP4 ratios were calculated as PV/non-PV. (**H**) Quantification and localization of AQP4 in the ventral cortex. Data were analysed with two-sided *t*-test. GM = grey matter; WM = white matter.

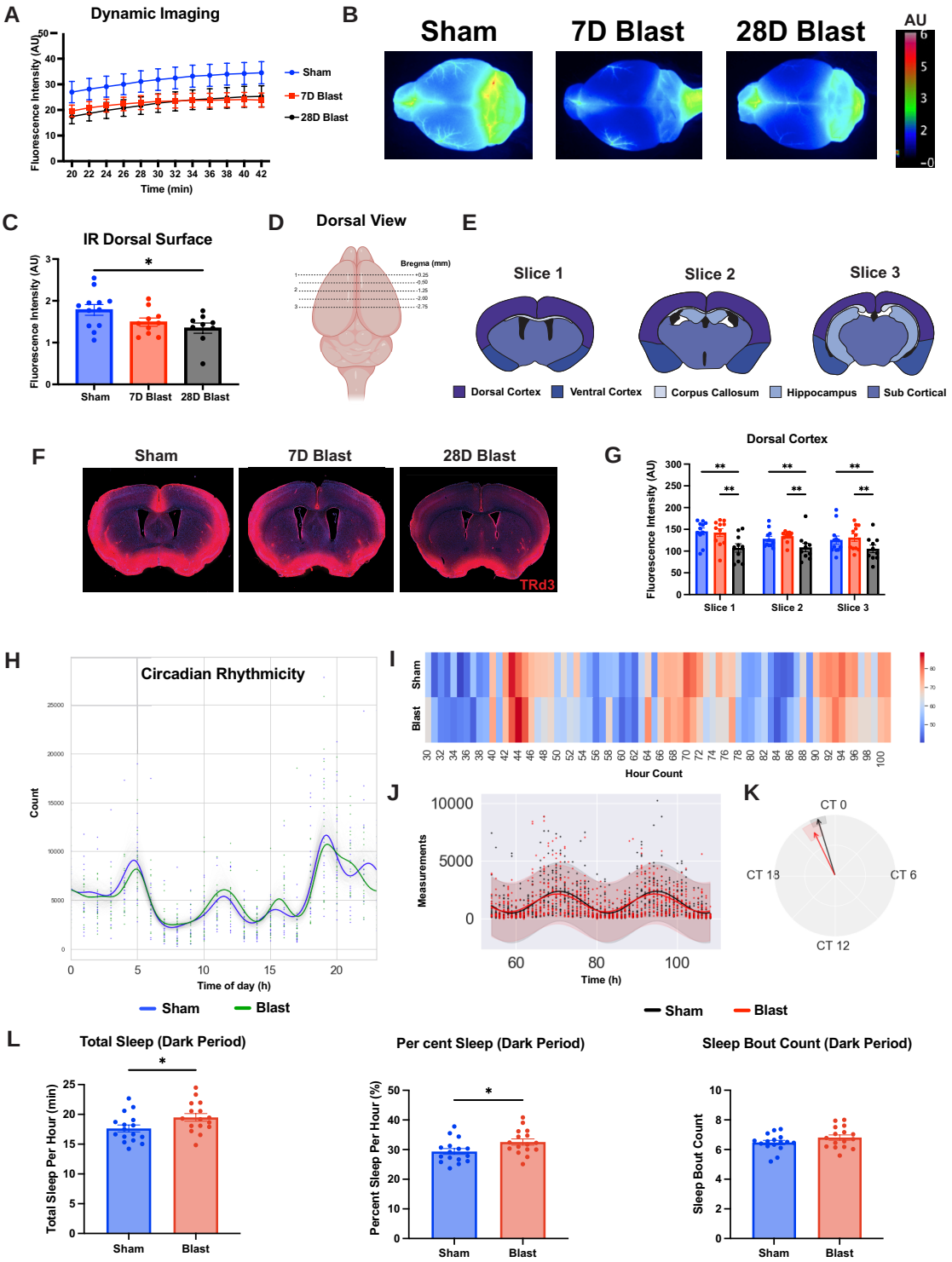

Figure 4 Delayed impairment of glymphatic influx and sleep-wake disruption in the murine blast-injured brain. (**A**) Quantification of the average cortical fluorescence intensity of *in vivo* dynamic transcranial images acquired every 2 min from 20 to 42 min following intracisternal tracer injection. Data are mean ± SEM from $n = 9$–12 mice/group and were analysed with two-way repeated measures ANOVA followed by Tukey's *post hoc* test. Main effects of Time (****$P < 0.0001$) and Time × Treatment interaction (***$P < 0.001$). (**B**) Representative *ex vivo* whole brain images of dorsal surface fluorescence taken following perfusion and removal from the skull. 7D Blast and 28D Blast = 7 and 28 days post mild repetitive blast traumatic brain injury. (**C**) Quantification of average fluorescence intensity of whole brain dorsal surface images. Data are mean ± SEM from $n = 9$–12 mice/group and were analysed with one-way ANOVA followed by Tukey's *post hoc* test (*$P < 0.05$). IR = infrared. (**D**) Diagram showing the range of the quantified coronal sections relative to bregma. (**E**) Diagram of the coronal sections and regions of interest across three quantified brain slices: dorsal cortex, ventral cortex, corpus callosum, hippocampus and subcortical regions. (**F**) Representative images of coronal brain sections at +0.25 mm from bregma showing Texas Red-conjugated dextran (3 kD) distribution within the brain. (**G**) Quantification of average fluorescence intensity of the dorsal cortex region across the three coronal sections between +0.25 mm to −2.75 mm from bregma. Data are mean ± SEM from $n = 10$ mice/group and were analysed with

(Continued)

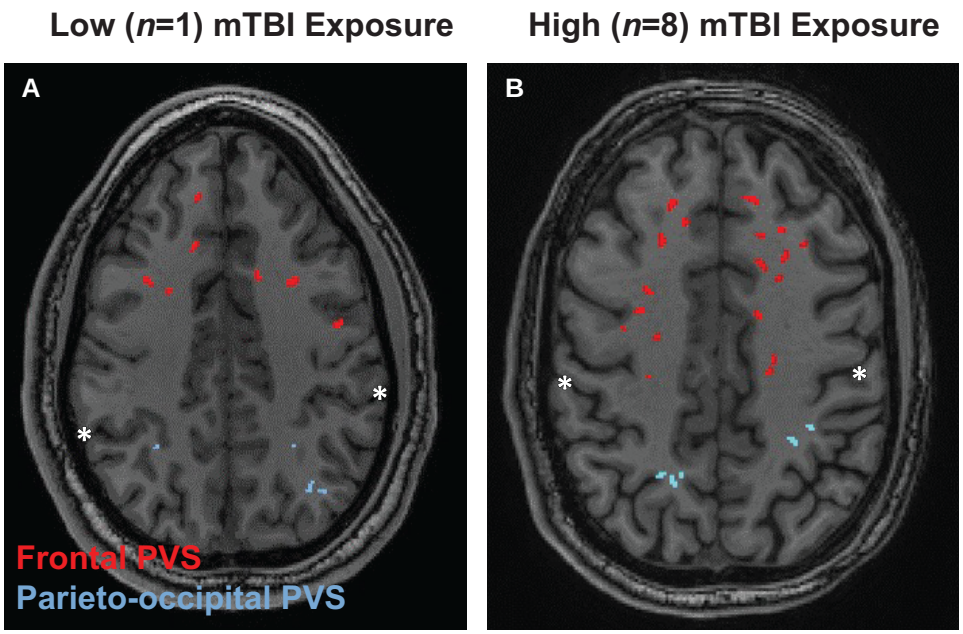

Figure 5 MRI visible perivascular spaces in human blast-injured veterans. T1-weighted MRI axial cut through the centrum semiovale (1-cm thick) in two age-matched subjects representative of the cohort. (**A**) Subject A had one mild traumatic brain injury (mTBI), whereas (**B**) Subject B had eight mTBIs. MRI-visible perivascular space (MV-PVS) burden was assessed using an automated algorithm. Frontal MV-PVSs, anterior to the central sulcus (asterisk) and parietal MV-PVSs, posterior to the central sulcus, are shown. Note the higher MV-PVS number in the frontal region detected by the algorithm in the subject with high blast mTBI exposure.

Table 1 Effects of number of mild traumatic brain injuries with loss of consciousness sustained in the military and effects of sleep on MRI-visible perivascular space burden

	Frontal		Temporal		Parieto-occipital	
	β (95% CI)	*P*	β (95% CI)	*P*	β (95% CI)	*P*
MV-PVS volume/cm^3 white matter[a]						
No. of mTBIs sustained in the military	0.12 (0.01–0.24)	**0.03**	0.04 (–0.05–0.15)	0.35	00.1 (0.003–0.23)	**0.04**
No. of mTBIs sustained in the military × Poor sleep	0.52 (0.06–0.1)	**0.02**	0.06 (–0.37–0.5)	0.76	0.46 (0.0004–0.93)	0.05
MV-PVS number/cm^3 white matter[a]						
No. of mTBIs sustained in the military	0.1 (0.001–0.2)	**0.04**	0.4 (–0.04–0.13)	0.31	0.1 (–0.01–0.24)	0.1
No. of mTBIs sustained in the military × Poor sleep	0.5 (0.06–0.9)	**0.02**	0.01 (–0.35–0.37)	0.31	0.64 (–0.2–1.5)	0.13

Data adjusted by age, systolic blood pressure and self-reported sleep quality (Pittsburgh Sleep Quality Inventory). Bold values = $P < 0.05$. CI = confidence interval; mTBI = mild traumatic brain injury; MV-PVS = MRI-visible perivascular space.
[a]MV-PVS data are log-transformed.

TBI, or alternatively whether longer post-blast intervals in populations of ageing veterans with blast TBI will permit such a clinical association to become evident. Addressing this important yet unresolved question will require the evaluation of AD- and CTE-related pathology in ageing veteran populations, perhaps using *in vivo* CSF- and PET-based biomarkers.

While much of the glymphatic literature has focused on the role of AQP4 and the glymphatic system in the clearance of pathological proteins such as amyloid-β and tau, this process also plays a role in the both the distribution and clearance of a variety of other solutes, including inflammatory cytokines, neuromodulators and metabolic substrates.[46-49] Following TBI, numerous brain-derived cytosolic proteins are transported through the brain to cervical lymphatics and into the blood via the glymphatic system,[18] further supporting the proposed role of the glymphatic system in distributing and clearing a wide array of compounds. Changes in these relatively unexplored glymphatic functions following blast TBI may underlie the multitude of post-traumatic symptoms and comorbidities associated with blast injury, including military PTSD, depression, anxiety, irritability, headache, sleep disturbances and cognitive impairment.[50] Supporting this notion, in our prior study of MRI data from a cohort of veterans of the Iraq and Afghanistan conflicts,

Figure 4 Continued
two-way ANOVA followed by Tukey's *post hoc* test (**$P < 0.01$). (**H**) Activity counts of Sham and blast-injured (Blast) mice measured using Comprehensive Lab Animal Monitoring (CLAM) chambers. (**I**) Heat map showing activity across time for Sham and Blast mice, starting at 6 a.m. on the second day in the CLAM chambers through 6 a.m. on the day they were removed. (**J**) Cosinor-based rhythmicity of sham and blast mice (**K**) Circadian rhythm acrophase shift of Blast versus Sham mice. (**L**) Quantification of total sleep, per cent sleep and sleep bout count for the dark 'waking' period measured from data collected in CLAM chambers. Data were analysed with two-sided *t*-test and are the mean ± SEM from $n = 16$ mice/group.

we reported that higher global numbers of MV-PVSs were associated with the persistence of a wide range of post-concussive symptoms, including dizziness, poor balance, poor coordination and vision problems, an average of 4–5 years following the last reported blast TBI.[32]

It is important to note that in our post-mortem cases, four of five Young Control and Blast TBI cases died by suicide, making PTSD and major depression important confounding variables to consider when discussing the observed changes in AQP4 expression and glymphatic function.[51] While a functional role for glymphatic impairment in psychiatric disorders has not yet been explored, major depressive disorder (MDD) has been shown to be associated with decreased AQP4 coverage at the perivascular endfoot in human post-mortem tissue from MDD cases[51] and in a mouse model of depression using chronic unpredictable mild stress.[52] AQP4 has also been shown to be required for the antidepressant action of fluoxetine.[53] TBI has a complex relationship with comorbid psychiatric conditions such as PTSD and depression, making it difficult to separate possible contributions of PTSD and depression to the observed post-traumatic changes in AQP4, or the effects of post-traumatic changes in AQP4 upon depression and PTSD. In addition, given the psychiatric conditions in the Young Controls, these controls may not represent a typical 'healthy' control population, as we were limited to the availability of specimens donated by former military service members, who tended to have psychiatric disorders. As such, the AQP4 and GFAP expression observed in the Young Controls may also have been influenced by the psychiatric disorders present. Given the psychiatric conditions present in both the Young Control and Blast TBI cases examined, the changes observed in the Blast cases may be underestimated compared to civilian controls with no psychiatric conditions; however, this remains to be elucidated.

In our mouse model of repetitive blast mTBI, we observed changes in circadian rhythm that are consistent with the daytime sleepiness and nighttime insomnia that have been reported in human participants following TBI. A retrospective study of soldiers returning from combat with mild to moderate TBIs (70.5% of which were blast TBIs) reported that 85.2% experienced excessive daytime sleepiness and 55.2% experienced insomnia.[54] Here we report a relationship between the MV-PVS burden (total number and volume) and the number of TBIs among veterans of the conflicts in Iraq and Afghanistan. Similarly, we found that this relationship is modulated by sleep quality, with poor sleepers exhibiting a steeper relationship between TBI number and MV-PVS burdens. Taken together, blast TBI and post-TBI sleep disturbances may act in a 'two hit' fashion that worsens glymphatic impairment. If true, then targeting sleep could be a therapeutic target to improve glymphatic function and patient outcomes following blast TBI. However, in light of the retrospective nature of this study, whether these participants may have had poor sleep before blast exposure or whether they developed poor sleep after blast TBI could not be determined. In addition, we were not able to measure MV-PVS in our blast mice, to compare to these human data, due to technical limitations associated with the small size of the mouse brain. One study has measured MV-PVS in a rat model of cerebral small vessel disease,[55] but measurement of MV-PVS in mice has not yet been proven possible with current technologies.

In the present study, while significant AQP4 changes were observed microscopically at the perivascular level surrounding capillaries across various laminae and regions, these changes appeared more subtle in comparison with the observed changes in global laminar AQP4 expression. Over the past 10 years, the glymphatic field has focused primarily on microscopic changes in perivascular AQP4 localization, with declining perivascular AQP4 localization and increasing non-perivascular AQP4 localization being associated with impaired glymphatic function in the setting of animal models of ageing, cerebrovascular injury and TBI,[9,15,56-58] as well as in human post-mortem ageing and case series of AD.[40,59] Consistent with these prior findings, in the present study, we report increased non-perivascular AQP4 localization surrounding capillaries in human post-mortem blast tissue and at 28 days post-injury in a mouse model of repetitive blast TBI. However, in contrast to these prior studies, we observed significant increases in perivascular AQP4 at the astroglial endfoot in the human blast-injured brain and a non-significant trend of increased perivascular AQP4 in the 28-day post blast murine brain as well. Because both perivascular and non-perivascular AQP4 immunofluorescence increased, we did not observe any changes in the 'AQP4 polarization' ratio, a measure similar to those used in prior studies. Although increasing perivascular AQP4 has been reported less often, this finding is not unique in the setting of brain injury or other neurological conditions. A similar increase in perivascular AQP4 in lesional areas of human post-mortem CTE brains was reported in a recent doctoral thesis.[60] Increased perivascular AQP4, with concomitant cortical astrogliosis, was also observed in human brain tissue from cases with idiopathic intracranial hypertension.[61] Human post-mortem tissue following focal ischaemic stroke exhibited reduced perivascular AQP4 in cortical astrocytes in ischaemic grey matter, but increased perivascular and non-perivascular AQP4 in ischaemic white matter.[62] Our findings, combined with the similar aforementioned finding of increased perivascular and non-perivascular AQP4 expression in white matter astrocytes in human post-mortem stroke tissue,[62] could suggest a unique response by white matter astrocytes to brain injury compared to grey matter astrocytes. Here it is noteworthy that in the present older controls, elevated AQP4 expression was observed in the white matter that was not paralleled by GFAP expression. AQP4 expression was also upregulated in the glial scar in a model of impact TBI.[15] The potential involvement of AQP4 in astrocyte migration and glial scar formation[63] may suggest the post-blast TBI alterations in AQP4 may not solely be a consequence of astrogliosis and interface scarring but may actively contribute to the initial formation of these processes. Overall, whether the AQP4 changes observed are the result, cause or a co-occurrence with this glial scarring is not known. It is likely a complex cascade in which the mechanisms that underlie astroglial scarring, including astrogliosis and neuroinflammatory signalling,[64] including transforming growth factors 1 (TGFβ-1) and 2 (TGFβ-2),[65] interleukin-1 (IL-1)[66] and inflammatory cytokines like interferon-γ (INFγ),[67] may also contribute to these AQP4 changes. Given that astroglial scarring does not occur in more mild head injury models[68,69] or in non-injury disease models where AQP4 changes are also observed,[41,57,59] we do not propose astroglial scarring to be the sole or main driver of AQP4 changes but rather that it may contribute to or co-occur with AQP4 changes in the setting of blast.

The striking laminar changes in AQP4 expression, particularly at the cortical surface and GM-WM boundary, may have important implications for post-traumatic changes in glymphatic CSF-ISF exchange and solute clearance. The pial surface and GM-WM interfaces are key entry and transition points for CSF and ISF movement into and through brain tissue. White matter tracts act as low-resistance, permissive pathways for dispersion or 'bulk-flow' movement of ISF,[70] while perivascular spaces surrounding penetrating blood vessels provide pathways for rapid fluid and solute exchange that may link subarachnoid CSF and white matter

fluid dynamics. It is possible that increased non-perivascular AQP4 in white matter astrocytes may make fluid movement through the typically anisotropic white matter more isotropic, slowing the movement of water along white matter tracts and leading to fluid stagnation. Given that the GM-WM interface is a boundary where ISF moves from higher resistance grey matter into typically low resistance white matter pathways, the observed interface scarring and widespread upregulation of AQP4 may exert a profound effect on fluid movement across this boundary and through brain tissue. Interestingly, a recent study in the gyrencephalic pig brain reported that cortical folds enhanced solute dispersion and that CSF tracer entered brain tissue at the sulci.[71] Following human blast exposure, we observed that AQP4 and GFAP enhancements were greatest at the sulcal depths, key sites of CSF entry into the brain. These observations are consistent with previous reports of greater histological injury at the sulcal depths in blast injury[72] and CTE,[73] and may have important implications for our understanding of the potential pathological link between blast TBI and CTE, in which the pathognomonic feature is the deposition of pathological tau at perivascular foci at the depths of sulci.

In a mouse model of impact moderate-severe TBI, the greatest impairment of glymphatic function and alterations in AQP4 localization were observed at 7 days post-TBI, while impaired glymphatic influx persisted for at least 28 days post-TBI.[9] In the present mouse model of repetitive blast injury, we observed that AQP4 expression and localization and CSF tracer influx were not significantly altered at Day 7 but were significantly altered at 28 days post-blast. This suggests that the pathophysiology and progression of blast TBI, characterized by a delayed but progressive impairment in glymphatic function, may fundamentally differ from that of impact TBI.

Studies combining both human and rodent data can help to bridge the gap from bench to bedside. In the present study, we were able to perform tracer studies in mice to understand changes in glymphatic function stemming from the AQP4 changes that we first observed in human tissue. The gold standard method for measuring glymphatic function in humans, intrathecal gadolinium injection, is invasive and is not performed unless clinically necessary, and less invasive imaging methods are currently in their infancy. Therefore, although rodent studies have their own limitations, when combined with human data, experiments in rodents can help to support and fill-in experimental gaps. Future studies combining human data and careful characterization of changes in AQP4 and glymphatic function in rodent models may help us to further understand the differences in pathophysiology and progression that present clinically in impact and blast TBI. Therapeutic targeting of glymphatic function to improve outcomes following blast TBI in both preclinical and clinical studies may also lead to improvements in clinical outcomes.

Overall, we report striking macroscopic laminar changes in AQP4 expression in the human and murine brain following blast TBI, which is associated with delayed glymphatic impairment. Correspondingly, in a cohort of military veterans blast TBI and poor sleep were associated with MV-PVS burden, a putative marker of perivascular glymphatic dysfunction. These findings suggest that alterations in AQP4 expression and impairment of glymphatic function following blast TBI may underlie the clinical linkage between blast TBI and the development of neurodegenerative conditions such as AD or CTE and may contribute to the development and persistence of post-concussive symptoms and comorbid neuropsychiatric conditions in veteran populations with blast TBI.

Data availability

Data are available on request.

Funding

We thank Dr Silbert at Oregon Health & Science University for providing the MV-PVS detection algorithm developed in her lab (Oregon Alzheimer's Research Center, grant P30AG066518). This work was supported by the National Heart, Lung and Blood Institute (NHLBI; K23HL150217-01), Department of Veterans Affairs Rehabilitation Research and Development Service Merit Review grant B77421 and National Institute on Aging (NIA; AG066518). The opinions and assertions expressed herein are those of the author(s) and do not reflect the official policy or position of the Uniformed Services University of the Health Sciences, Department of Defense or Veteran's Administration.

Competing interests

J.J.I. serves as the Chair of the Scientific Advisory Board for Applied Cognition, Inc., from which he receives compensation and in which he holds an equity stake. The other authors report no competing interests.

Supplementary material

Supplementary material is available at *Brain* online.

References

1. Taber KH, Warden DL, Hurley RA. Blast-related traumatic brain injury: What is known? *J Neuropsychiatry Clin Neurosci*. 2006;18:141-145.
2. Miller ST, Cooper CF, Elsbernd P, et al. Localizing clinical patterns of blast traumatic brain injury through computational modeling and simulation. *Front Neurol*. 2021;12:547655.
3. Martindale SL, Ord AS, Rule LG, et al. Effects of blast exposure on psychiatric and health symptoms in combat veterans. *J Psychiatr Res*. 2021;143:189-195.
4. Hostetter TA, Hoffmire CA, Forster JE, et al. Suicide and traumatic brain injury among individuals seeking veterans health administration services between fiscal years 2006 and 2015. *J Head Trauma Rehabil*. 2019;34:E1-E9.
5. Weiner MW, Friedl KE, Pacifico A, et al. Military risk factors for Alzheimer's disease. *Alzheimers Dement*. 2013;9:445-451.
6. Iliff JJ, Wang M, Liao Y, et al. A paravascular pathway facilitates CSF flow through the brain parenchyma and the clearance of interstitial solutes, including amyloid β. *Sci Transl Med*. 2012;4:147ra111-147ra111.
7. Iliff JJ, Lee H, Yu M, et al. Brain-wide pathway for waste clearance captured by contrast-enhanced MRI. *J Clin Invest*. 2013;123:1299-1309.
8. Xie L, Kang H, Xu Q, et al. Sleep drives metabolite clearance from the adult brain. *Science*. 2013;342:373-377.
9. Iliff JJ, Chen MJ, Plog BA, et al. Impairment of glymphatic pathway function promotes tau pathology after traumatic brain injury. *J Neurosci*. 2014;34:16180-16193.
10. Ishida K, Yamada K, Nishiyama R, et al. Glymphatic system clears extracellular tau and protects from tau aggregation and neurodegeneration. *J Exp Med*. 2022;219:e20211275.

11. Zhang Y, Zhang C, He XZ, et al. Interaction between the glymphatic system and α-synuclein in Parkinson's disease. *Mol Neurobiol*. 2023;60:2209-2222.
12. Iliff JJ, Wang M, Zeppenfeld DM, et al. Cerebral arterial pulsation drives paravascular CSF-interstitial fluid exchange in the murine brain. *J Neurosci*. 2013;33:18190-18199.
13. Mestre H, Tithof J, Du T, et al. Flow of cerebrospinal fluid is driven by arterial pulsations and is reduced in hypertension. *Nat Commun*. 2018;9:4878.
14. Mestre H, Hablitz LM, Xavier ALR, et al. Aquaporin-4-dependent glymphatic solute transport in the rodent brain. *eLife*. 2018;7:e40070.
15. Ren Z, Iliff JJ, Yang L, et al. 'Hit & run' model of closed-skull traumatic brain injury (TBI) reveals complex patterns of post-traumatic AQP4 dysregulation. *J Cereb Blood Flow Metab*. 2013;33:834-845.
16. Christensen J, Wright DK, Yamakawa GR, et al. Repetitive mild traumatic brain injury alters glymphatic clearance rates in limbic structures of adolescent female rats. *Sci Rep*. 2020;10:6254.
17. Zhang E, Wan X, Yang L, et al. Omega-3 polyunsaturated fatty acids alleviate traumatic brain injury by regulating the glymphatic pathway in mice. *Front Neurol*. 2020;11:707.
18. Plog BA, Dashnaw ML, Hitomi E, et al. Biomarkers of traumatic injury are transported from brain to blood via the glymphatic system. *J Neurosci*. 2015;35:518-526.
19. Gu W, Bai Y, Cai J, et al. Hypothermia impairs glymphatic drainage in traumatic brain injury as assessed by dynamic contrast-enhanced MRI with intrathecal contrast. *Front Neurosci*. 2023;17:1061039.
20. Li L, Chopp M, Ding G, et al. MRI detection of impairment of glymphatic function in rat after mild traumatic brain injury. *Brain Res*. 2020;1747:147062.
21. Shively SB, Horkayne-Szakaly I, Jones RV, et al. Characterisation of interface astroglial scarring in the human brain after blast exposure: A post-mortem case series. *Lancet Neurol*. 2016;15:944-953.
22. Bankhead P, Loughrey MB, Fernández JA, et al. Qupath: Open source software for digital pathology image analysis. *Sci Rep*. 2017;7:16878.
23. Huber BR, Meabon JS, Martin TJ, et al. Blast exposure causes early and persistent aberrant phospho- and cleaved-tau expression in a murine model of mild blast-induced traumatic brain injury. *J Alzheimers Dis*. 2013;37:309-323.
24. Schindler AG, Meabon JS, Pagulayan KF, et al. Blast-related disinhibition and risk seeking in mice and combat veterans: Potential role for dysfunctional phasic dopamine release. *Neurobiol Dis*. 2017;106:23-34.
25. Keil SA, Braun M, O'Boyle R, et al. Dynamic infrared imaging of cerebrospinal fluid tracer influx into the brain. *Neurophotonics*. 2022;9:031915.
26. Pack AI, Galante RJ, Maislin G, et al. Novel method for high-throughput phenotyping of sleep in mice. *Physiol Genomics*. 2007;28:232-238.
27. Velikajne N, Moškon M. RhythmCount: A python package to analyse the rhythmicity in count data. *J Comput Sci*. 2022;63:101758.
28. Moškon M. Cosinorpy: A python package for cosinor-based rhythmometry. *BMC Bioinformatics*. 2020;21:485.
29. Pagulayan KF, Petrie EC, Cook DG, et al. Effect of blast-related mTBI on the working memory system: A resting state fMRI study. *Brain Imaging Behav*. 2020;14:949-960.
30. Pagulayan KF, Rau H, Madathil R, et al. Retrospective and prospective memory among OEF/OIF/OND veterans with a self-reported history of blast-related mTBI. *J Int Neuropsychol Soc*. 2018;24:324-334.
31. Petrie EC, Cross DJ, Yarnykh VL, et al. Neuroimaging, behavioral, and psychological sequelae of repetitive combined blast/impact mild traumatic brain injury in Iraq and Afghanistan war veterans. *J Neurotrauma*. 2014;31:425-436.
32. Piantino J, Schwartz DL, Luther M, et al. Link between mild traumatic brain injury, poor sleep, and magnetic resonance imaging: Visible perivascular spaces in veterans. *J Neurotrauma*. 2021;38:2391-2399.
33. Buysse DJ, Reynolds CF III, Monk TH, et al. The Pittsburgh sleep quality Index: A new instrument for psychiatric practice and research. *Psychiatry Res*. 1989;28:193-213.
34. Boespflug EL, Schwartz DL, Lahna D, et al. MR Imaging-based multimodal autoidentification of perivascular spaces (mMAPS): Automated morphologic segmentation of enlarged perivascular spaces at clinical field strength. *Radiology*. 2018;286:632-642.
35. Schwartz DL, Boespflug EL, Lahna DL, et al. Autoidentification of perivascular spaces in white matter using clinical field strength T(1) and FLAIR MR imaging. *Neuroimage*. 2019;202:116126.
36. Piantino J, Boespflug EL, Schwartz DL, et al. Characterization of MR imaging–visible perivascular spaces in the white matter of healthy adolescents at 3 T. *Am J Neuroradiol*. 2020;41:2139.
37. Hablitz LM, Plá V, Giannetto M, et al. Circadian control of brain glymphatic and lymphatic fluid flow. *Nat Commun*. 2020;11:4411.
38. Potter GM, Chappell FM, Morris Z, et al. Cerebral perivascular spaces visible on magnetic resonance imaging: Development of a qualitative rating scale and its observer reliability. *Cerebrovasc Dis*. 2015;39(3-4):224-231.
39. Pedersen TJ, Keil SA, Han W, et al. The effect of aquaporin-4 mis-localization on aβ deposition in mice. *Neurobiol Dis*. 2023;181:106100.
40. Simon M, Wang MX, Ismail O, et al. Loss of perivascular aquaporin-4 localization impairs glymphatic exchange and promotes amyloid β plaque formation in mice. *Alzheimers Res Ther*. 2022;14:59.
41. Harrison IF, Ismail O, Machhada A, et al. Impaired glymphatic function and clearance of tau in an Alzheimer's disease model. *Brain*. 2020;143:2576-2593.
42. Priemer DS, Iacono D, Rhodes CH, et al. Chronic traumatic encephalopathy in the brains of military personnel. *N Engl J Med*. 2022;386:2169-2177.
43. Ryu J, Horkayne-Szakaly I, Xu L, et al. The problem of axonal injury in the brains of veterans with histories of blast exposure. *Acta Neuropathol Commun*. 2014;2:153.
44. Goldstein LE, Fisher AM, Tagge CA, et al. Chronic traumatic encephalopathy in blast-exposed military veterans and a blast neurotrauma mouse model. *Sci Transl Med*. 2012;4:134ra60.
45. Omalu B, Hammers JL, Bailes J, et al. Chronic traumatic encephalopathy in an Iraqi war veteran with posttraumatic stress disorder who committed suicide. *Neurosurg Focus*. 2011;31:E3.
46. Lundgaard I, Lu ML, Yang E, et al. Glymphatic clearance controls state-dependent changes in brain lactate concentration. *J Cereb Blood Flow Metab*. 2017;37:2112-2124.
47. Lundgaard I, Li B, Xie L, et al. Direct neuronal glucose uptake heralds activity-dependent increases in cerebral metabolism. *Nat Commun*. 2015;6:6807.
48. Rangroo Thrane V, Thrane AS, Plog BA, et al. Paravascular microcirculation facilitates rapid lipid transport and astrocyte signaling in the brain. *Sci Rep*. 2013;3:2582.
49. Rasmussen MK, Mestre H, Nedergaard M. Fluid transport in the brain. *Physiol Rev*. 2022;102:1025-1151.
50. VA/DoD clinical practice guideline for management of concussion/mild traumatic brain injury. *J Rehabil Res Dev*. 2009. 46: Cp1-C68.
51. Rajkowska G, Hughes J, Stockmeier CA, et al. Coverage of blood vessels by astrocytic endfeet is reduced in major depressive disorder. *Biol Psychiatry*. 2013;73:613-621.
52. Xia M, Yang L, Sun G, et al. Mechanism of depression as a risk factor in the development of Alzheimer's disease: The function

of AQP4 and the glymphatic system. *Psychopharmacology (Berl)*. 2017;234:365-379.
53. Kong H, Sha L-l, Fan Y, et al. Requirement of AQP4 for antidepressive efficiency of fluoxetine: Implication in adult hippocampal neurogenesis. *Neuropsychopharmacology*. 2009;34:1263-1276.
54. Collen J, Orr N, Lettieri CJ, et al. Sleep disturbances among soldiers with combat-related traumatic brain injury. *Chest*. 2012; 142:622-630.
55. Monte B, Constantinou S, Koundal S, et al. Characterization of perivascular space pathology in a rat model of cerebral small vessel disease by in vivo magnetic resonance imaging. *J Cereb Blood Flow Metab*. 2022;42:1813-1826.
56. Wang M, Ding F, Deng S, et al. Focal solute trapping and global glymphatic pathway impairment in a murine model of multiple microinfarcts. *J Neurosci*. 2017;37:2870-2877.
57. Kress BT, Iliff JJ, Xia M, et al. Impairment of paravascular clearance pathways in the aging brain. *Ann Neurol*. 2014;76:845-861.
58. Wang M, Iliff JJ, Liao Y, et al. Cognitive deficits and delayed neuronal loss in a mouse model of multiple microinfarcts. *J Neurosci*. 2012;32:17948-17960.
59. Zeppenfeld DM, Simon M, Haswell JD, et al. Association of perivascular localization of aquaporin-4 with cognition and Alzheimer disease in aging brains. *JAMA Neurol*. 2017;74:91-99.
60. Babcock KJ. Histopathological assessment of atroglial aquaporin-4 expression in chronic traumatic encephalopathy. PhD thesis. The University of Boston, School of Medicine; 2018. https://hdl.handle.net/2144/30913
61. Eide PK, Eidsvaag VA, Nagelhus EA, et al. Cortical astrogliosis and increased perivascular aquaporin-4 in idiopathic intracranial hypertension. *Brain Res*. 2016;1644:161-175.
62. Stokum JA, Mehta RI, Ivanova S, et al. Heterogeneity of aquaporin-4 localization and expression after focal cerebral ischemia underlies differences in white versus grey matter swelling. *Acta Neuropathol Commun*. 2015;3:61.
63. Saadoun S, Papadopoulos MC, Watanabe H, et al. Involvement of aquaporin-4 in astroglial cell migration and glial scar formation. *J Cell Sci*. 2005;118(Pt 24):5691-5698.
64. Adams KL, Gallo V. The diversity and disparity of the glial scar. *Nat Neurosci*. 2018;21:9-15.
65. Moon LDF, Fawcett JW. Reduction in CNS scar formation without concomitant increase in axon regeneration following treatment of adult rat brain with a combination of antibodies to TGFβ1 and β2. *Eur J Neurosci*. 2001;14:1667-1677.
66. Giulian D, Woodward J, Young DG, et al. Interleukin-1 injected into mammalian brain stimulates astrogliosis and neovascularization. *J Neurosci*. 1988;8:2485-2490.
67. Yong VW, Moumdjian R, Yong FP, et al. Gamma-interferon promotes proliferation of adult human astrocytes in vitro and reactive gliosis in the adult mouse brain in vivo. *Proc Natl Acad Sci U S A*. 1991;88:7016-7020.
68. Shandra O, Winemiller AR, Heithoff BP, et al. Repetitive diffuse mild traumatic brain injury causes an atypical astrocyte response and spontaneous recurrent seizures. *J Neurosci*. 2019; 39:1944-1963.
69. Anderson MA, Ao Y, Sofroniew MV. Heterogeneity of reactive astrocytes. *Neurosci Lett*. 2014;565:23-29.
70. Rosenberg GA, Kyner WT, Estrada E. Bulk flow of brain interstitial fluid under normal and hyperosmolar conditions. *Am J Physiol*. 1980;238:F42-F49.
71. Bèchet NB, Shanbhag NC, Lundgaard I. Glymphatic pathways in the gyrencephalic brain. *J Cereb Blood Flow Metab*. 2021;41: 2264-2279.
72. McKee AC, Robinson ME. Military-related traumatic brain injury and neurodegeneration. *Alzheimers Dement*. 2014;10(3S): S242-S253.
73. Fagan BT, Satapathy SS, Rutledge JN, et al. Simulation of the strain amplification in Sulci due to blunt impact to the head. *Front Neurol*. 2020;11:998.